nature nanotechnology

SUPPLEMENTARY INFORMATION

DOI: 10.1038/NNANO.2011.183

Formation of droplet networks that function in aqueous environments

Gabriel Villar, Andrew J. Heron and Hagan Bayley

Supplementary discussions

Supplementary Discussion 1:
Incubation time and oils

It was essential to wait several minutes (the *incubation* time) before encapsulation. If transferred too soon into the oil drop, the aqueous droplets fused with each other and with the external aqueous phase. The incubation time may be required for well-packed lipid monolayers to form around the oil drop and aqueous droplets [1].

In most of the foreseen applications, multisomes should be approximately neutrally buoyant in water, and the silicone oil used was chosen accordingly for its density of 1.01 g cm^{-3}. Equally important, however, was the minimum incubation time required to form stable multisomes with a given oil: whereas this was < 5 min for the silicone oil and hexadecane mixture containing 0.2 mg ml^{-1} 1,2-diphytanoyl-*sn*-glycero-3-phosphocholine (DPhPC), multisomes made with 1-bromododecane (density 1.04 g cm^{-3}) were not stable even after longer incubation times and at higher lipid concentrations.

Supplementary Discussion 2:
Prediction of the geometry of multisomes with several inner droplets

The analysis presented here may be extended to predict the metastable geometry of a multisome with several inner droplets. As well as becoming more algebraically involved, the analysis must then account for all the locally stable configurations available to the inner droplets. For instance, three aqueous droplets encapsulated in a single multisome were observed to settle in either a linear or triangular arrangement, depending on the droplets' positions and velocities at the moment of encapsulation. One must also account for transitions between locally stable states, as an encapsulated droplet network in one configuration may change to another, even after the formation of internal and external bilayers. In multisomes with three inner droplets settled in a linear arrangement, having formed internal and external bilayers, the inner droplets have been observed to then slide along the surface of the oil drop to irreversibly adopt the triangular configuration.

Therefore the following two criteria must be fulfilled in order to produce a multisome with its inner droplets in a particular desired arrangement:

1. The desired arrangement should be a metastable state. This corresponds to a well in the energy landscape, and the depth of the well determines the robustness of the state to perturbations. Some states, such as a linear arrangement of three inner droplets, are not very stable to perturbation and therefore are not reliable designs for encapsulated droplet

networks. It may be possible to stabilize such states by the addition of auxiliary inner droplets, so that locally unstable designs may be realized within larger, locally stable arrangements.

2. The desired arrangement should be accessible from the droplets' initial trajectories at the moment of encapsulation. If the desired arrangement corresponds to the only minimum of the energy landscape, the inner droplets will adopt the arrangement regardless of their initial trajectories. However, if multiple metastable geometries exist then the final arrangement adopted will depend on the initial trajectories of the droplets, and on the shape of the energy landscape. In this case, the design of complex multisomes with a particular desired geometry would require either a highly reproducible means of encapsulation, or some means of driving the inner droplets from one metastable state to another.

Supplementary Discussion 3:
Origin of the delay between addition of Ca^{2+} and fluorescence increase

The fluorescence measurements showed a time lag between the start of Ca^{2+} flux and a fluorescence increase. This is due to competitive binding of Ca^{2+} by EDTA, included in the inner droplets to chelate the small amount of contaminating Ca^{2+} present in the buffer salt, which would otherwise have produced background fluorescence. Ca^{2+} binds to fluo-4 and EDTA at similar rates ($k_{on} \sim 10^7 - 10^8\,M^{-1}\,s^{-1}$), but dissociates from fluo-4 much more rapidly than from EDTA, with $k_{off} \sim 400\,s^{-1}$ and $< 1\,s^{-1}$, respectively [2, 3]. On a timescale of minutes, therefore, the EDTA acts as a sink for almost all the Ca^{2+} in the droplet, and only once the EDTA has been saturated can a significant proportion of the fluo-4 molecules bind Ca^{2+} ions.

Supplementary Discussion 4:
Choice of lipid mixture for temperature-sensitive multisomes

Attempts to form multisomes with 1,2-dipalmitoyl-*sn*-glycero-3-phosphocholine (DPPC) (melting transition temperature $T_m = 41\,°C$), popularly used for temperature-sensitive liposomes, did not yield stable bilayers when performed over a range of lipid concentrations and incubation times. The instability of giant DPPC liposomes has been noted elsewhere [4, 5]. However, multisomes made with a 1:1 (mol/mol) mixture of DPPC and DPhPC were stable, with $\sim$90% surviving for at least 12 h ($n = 8$). When subjected to a temperature gradient, the external bilayers of multisomes made with this lipid mixture with a single inner droplet ruptured suddenly at $32.6 \pm 1.6\,°C$ ($n = 11$), releasing the contents of the inner droplets into the external aqueous solution. The bursting temperature did not show a significant trend as the molar proportion of DPhPC was varied from $\sim 15 - 75\%$, and significantly lower proportions of DPhPC failed to stabilize the bilayers.

That the bursting temperature is considerably lower than the transition temperature of DPPC is likely due to two factors. First, the addition of DPhPC to DPPC is known to significantly broaden the melting transition, and to decrease the peak transition temperature [6]. Second, larger temperature-sensitive liposomes have been shown to release their contents at lower temperatures than smaller liposomes [7, 8]. This size effect, combined with the early onset of the melting transition caused by the addition of DPhPC, could account for the dramatic disruption of the bilayer observed well below the T_m of pure DPPC.

Following the hypothesis that lipids similar to DPPC suffer a similar broadening of the melting transition upon the admixture of DPhPC, DPPC was replaced by 1,2-distearoyl-*sn*-glycero-3-phosphocholine (DSPC) ($T_m \approx 55\,°C$) in order to raise the bursting temperature of

multisomes to within a range appropriate for clinical mild hyperthermia, with a view toward developing the potential of multisomes as drug delivery vehicles.

Supplementary Discussion 5:
Effect of finite curvature on multisomal monolayers and bilayers

Some properties of multisomes, such as the phase transitions of the monolayers and bilayers, are likely to depend on the curvatures of these interfaces for multisomes smaller than $\sim$1 μm in diameter [9]. Such properties could be tailored in various ways [10], for example by the use of lipids with high "curvature", that is, lipids that form bilayers with high intrinsic curvature. For instance, sub-μm-diameter multisomes might be stabilized by coating the encapsulated droplets and the oil drop with lipids of opposite curvature. This might be achieved by incubating the aqueous droplets in oil containing lipids with negative curvature, then transferring the droplets into an incubated oil drop coated with a monolayer of lipid with positive curvature.

Supplementary Discussion 6:
Miniaturization of multisomes by microfluidics

Previous studies have encapsulated aqueous droplets in $\sim$100-μm diameter oil drops (stabilized by surfactants or block copolymers) in bulk aqueous solution, by consecutive shearing [11] or flow-focusing [12, 13] of aqueous and oil flows. In a recent study [14], the flow-focusing method was used to create groups of aqueous droplets joined by bilayers of block copolymers. These droplet aggregates are structurally similar to multisomes, and the same microfluidic technique should be capable of producing $\sim$100-μm diameter structurally-defined multisomes with functional bilayer interfaces as presented here. The use of lipids, as opposed to alternative interfacial stabilizing agents, allows multisomes to be functionalized based on the richly varied properties of bilayers and membrane proteins.

Supplementary Methods

1 Derivation of the free energy landscape of a multisome with a single inner droplet

1.1 Definitions and assumptions

Let the radius of the oil drop, without the aqueous droplet inside, be R_1, and the radius of the aqueous droplet be R_2. Once the bilayer has formed, we assume that each of the two monolayers and the bilayer minimize their own surface areas, so that the oil drop and aqueous droplet may be constructed from spherical caps (Fig. 1). This assumption is validated by photomicrographs of multisomes with single inner droplets, such as Fig. 1c of the main text. The geometry of the spherical caps is defined by the contact angles relative to the horizontal θ_i, and radii of curvature r_i, where $i = 1, 2, 3$. A similar parameterization has been used for vesicles containing phase-separated aqueous solutions [15], which are physically distinct from multisomes but mathematically equivalent under certain conditions.

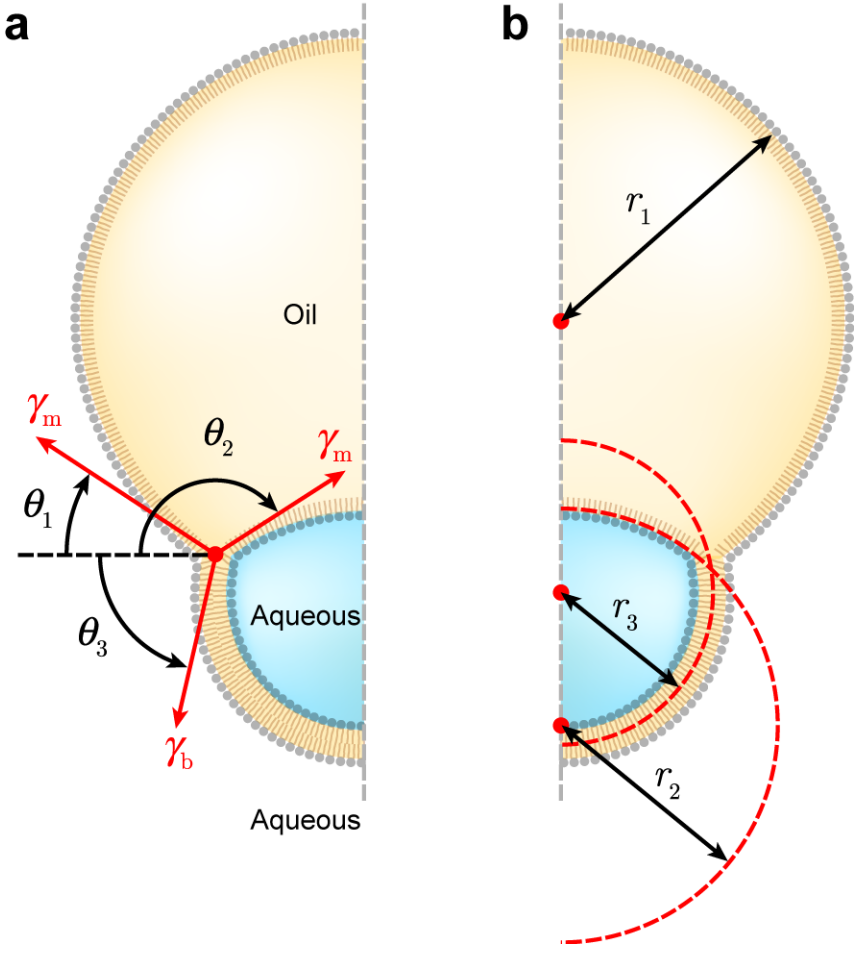

Figure 1: Geometrical definitions. (a) Contact angles θ_i, defined relative to the horizontal. (b) Radii of curvature r_i.

We assume that the multisome has two types of interface: lipid monolayers, with surface tension γ_m; and a lipid bilayer, with surface tension γ_b. As shown in the Appendix, surface

tension forces are expected to be ∼60 times greater than buoyancy forces, which were therefore taken to be negligible. Both monolayer and bilayer surface tensions were assumed to be independent of curvature at the very low curvatures investigated here (radius of curvature $> 50\,\mu$m, corresponding to curvature $< 0.02\,\mu\text{m}^{-1}$).

1.2 Free energies

When the aqueous droplet contacts the edge of the oil drop to form a bilayer, there is a free energy change that comprises two contributions. The first is a favourable component from the joining of two monolayers to form a bilayer. The second is an unfavourable component from distortion of the monolayer-covered surfaces. That the second necessarily occurs can be seen by considering that the initial spherical geometries of the oil drop and aqueous droplet have minimal surface area per unit volume, and that their volume remains constant during the formation of the bilayer; it follows that any distortion of their geometry will incur an increase in surface area.

Here we aim to calculate the balance of these two contributions for any given geometry, thereby producing a free energy landscape, in the space of all possible geometries, for the formation of an encapsulated droplet bilayer. The minimum of this landscape represents a state that is only kinetically stable, or metastable, as fusion of the inner droplets with the bulk aqueous phase would further decrease the free energy of the system.

1.2.1 Initial state

The initial state of the system consists of the monolayer-coated aqueous droplet in the monolayer-coated oil drop, prior to the formation of a bilayer. Recalling that surface tension is surface energy per unit area, the surface energy of this system is given by the surface tension of each surface multiplied by its area. From our earlier definitions, the initial free energy is then:

$$F_{\text{initial}} = \gamma_{\text{m}} \left(A_1 + A_2 \right), \tag{1}$$

where $A_i = 4\pi R_i^2$ with $i = 1, 2$ are the initial areas of the oil drop and aqueous droplet, respectively.

1.2.2 Final state

In the final state of the system, a portion of the aqueous droplet has contacted the surface of the oil drop to form a bilayer. As before, the free energy of this state is simply given by the surface tension of each surface multiplied by its area. The final free energy is therefore:

$$F_{\text{final}} = \gamma_{\text{m}} \left(a_1 + a_2 \right) + \gamma_{\text{b}} a_3, \tag{2}$$

where a_i with $i = 1, 2, 3$ are the areas of the spherical caps forming the surfaces with radii of curvature r_i. In the Appendix it is shown that the area of each spherical cap is given by: $a_i = 2\pi r_i^2 \left(1 + \cos\theta_i\right)$.

1.2.3 Free energy change

Taking the difference between the free energies of the final (Eq. 2) and initial (Eq. 1) states, we obtain the free energy of formation of a multisome bilayer:

$$\Delta F = \gamma_{\text{m}} \left(a_1 + a_2 \right) + \gamma_{\text{b}} a_3 - \gamma_{\text{m}} \left(A_1 + A_2 \right).$$

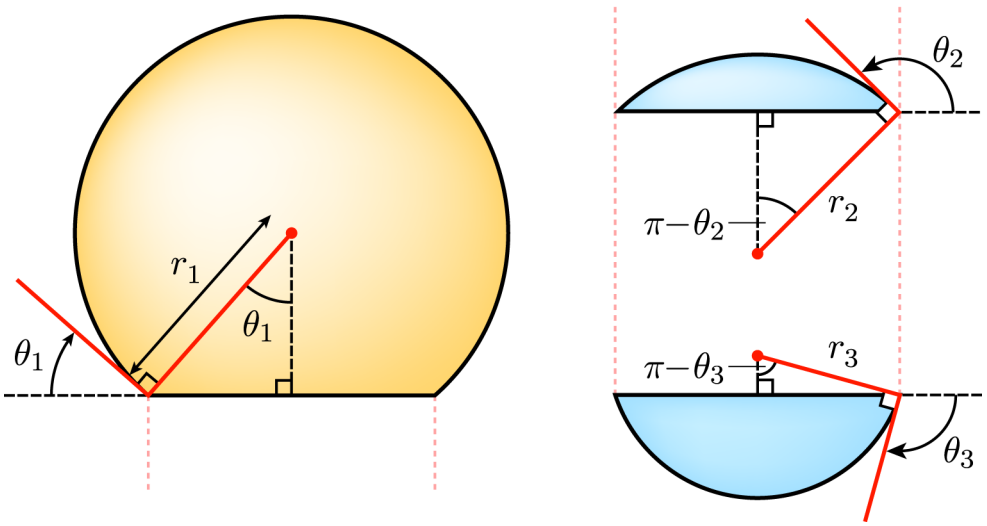

Figure 2: Edge matching.

Substituting our expressions for the A_i and a_i and rearranging, this becomes:

$$\Delta F = 2\pi\gamma_{\mathrm{m}}\left[r_1^2\left(1+\cos\theta_1\right)+r_2^2\left(1+\cos\theta_2\right)+\frac{\gamma_{\mathrm{b}}}{\gamma_{\mathrm{m}}}r_3^2\left(1+\cos\theta_3\right)-2\left(R_1^2+R_2^2\right)\right].$$

In the Appendix it is shown that the ratio between the bilayer and monolayer surface tensions can be expressed in terms of the contact angle of a droplet interface bilayer in bulk oil, θ_{c}, as: $\gamma_{\mathrm{b}}/\gamma_{\mathrm{m}} = 2\cos\theta_{\mathrm{c}}$. Using this result in the above expression, we obtain:

$$\Delta F = 2\pi\gamma_{\mathrm{m}}\left[r_1^2\left(1+\cos\theta_1\right)+r_2^2\left(1+\cos\theta_2\right)+2\cos\theta_c r_3^2\left(1+\cos\theta_3\right)-2\left(R_1^2+R_2^2\right)\right]. \quad (3)$$

1.3 Constraints

At this point we are able to calculate the free energy of bilayer formation for an encapsulated droplet with a given geometry. In other words, we can compute ΔF for a given set of initial conditions (R_1, R_2) and final conditions $(r_1, r_2, r_3, \theta_1, \theta_2, \theta_3)$. However, not all final conditions are possible for a given encapsulated droplet: if the values of R_1 and R_2 are fixed, after forming the bilayer not every combination of the r_i and θ_i is accessible. For instance, some combinations of values would result in the volume of oil being greater after bilayer formation than before. The θ_i are therefore not free variables, and it is now necessary to impose some constraints on the system[1].

1.3.1 Edge matching

The first constraint we apply is that the various spherical caps must coincide at their edges. As illustrated in Fig. 2, this implies that the circles that cap the truncated spheres must all have the same diameter. With reference to this figure, and recalling that $\sin\theta = \sin\left(\pi-\theta\right)$,

[1] A geometrical interpretation of the imposition of constraints is as follows. Each constraint that we apply in the form of an equation defines some subset of the $(r_1, r_2, r_3, \theta_1, \theta_2, \theta_3)$ space, for instance some volume or surface. The intersection of all these subsets (that is, where the subsets overlap) define the region in the parameter space accessible to a given multisome.

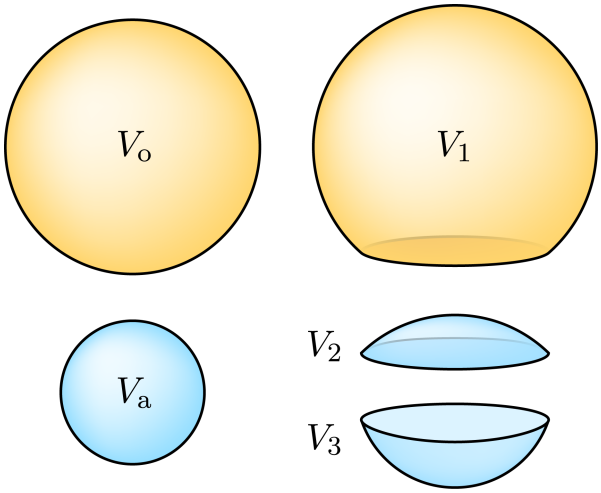

Figure 3: Volumes of spherical caps.

the following two conditions are straightforwardly derived:

$$r_1 \sin\theta_1 = r_2 \sin\theta_2; \tag{4}$$
$$r_2 \sin\theta_2 = r_3 \sin\theta_3. \tag{5}$$

1.3.2 Volume conservation

The second constraint we apply is the conservation of the volumes of the oil drop and aqueous droplet. We denote the oil volume by V_o, the volume of the aqueous droplet by V_a, and the volumes of the three spherical caps comprising the encapsulated droplet after bilayer formation by V_1, V_2 and V_3 as in Fig. 3. Conservation of oil volume then yields: $V_\mathrm{o} = V_1 - V_2$. Recalling the definition of R_1, we know that $V_\mathrm{o} = \frac{4\pi}{3} R_1^3$, so that this volume conservation equation becomes:

$$\frac{4\pi}{3} R_1^3 = V_1 - V_2. \tag{6}$$

Similarly, conservation of volume for the aqueous droplet implies: $V_\mathrm{a} = V_2 + V_3$. Using $V_\mathrm{a} = \frac{4\pi}{3} R_2^3$, this becomes:

$$\frac{4\pi}{3} R_2^3 = V_2 + V_3. \tag{7}$$

In the Appendix it is shown that the volume of a spherical cap with radius of curvature r_i and contact angle θ_i, as defined in Fig. 1, is:

$$V_i = \frac{\pi r_i^3}{12} \left(8 - \cos 3\theta_i + 9\cos\theta_i\right).$$

For brevity, we define the function

$$\alpha(\theta) = 8 - \cos 3\theta + 9\cos\theta, \tag{8}$$

so that:

$$V_i = \frac{\pi r_i^3}{12} \alpha(\theta_i). \tag{9}$$

Substituting this expression for each V_i in the volume conservation equation for the oil drop, Eq. 6, we obtain:

$$\frac{4\pi}{3}R_1^3 = \frac{\pi r_1^3}{12}\,\alpha(\theta_1) - \frac{\pi r_2^3}{12}\,\alpha(\theta_2)$$

$$\implies 16R_1^3 = r_1^3\,\alpha(\theta_1) - r_2^3\,\alpha(\theta_2)\,. \tag{10}$$

Similarly, the volume conservation equation for the aqueous droplet, Eq. 7, becomes:

$$\frac{4\pi}{3}R_1^3 = \frac{\pi r_2^3}{12}\,\alpha(\theta_2) + \frac{\pi r_3^3}{12}\,\alpha(\theta_3)$$

$$\implies 16R_2^3 = r_2^3\,\alpha(\theta_2) + r_3^3\,\alpha(\theta_3)\,. \tag{11}$$

1.4 Solving the equations

To summarize the progress so far: we have an expression, Eq. 3, for the free energy of formation of an encapsulated droplet, initially consisting of an oil drop of given radius R_1 that contains an aqueous droplet of given radius R_2, and finally having geometric parameters r_i and θ_i:

$$\Delta F = 2\pi\gamma_{\mathrm{m}}\left[r_1^2\,(1+\cos\theta_1) + r_2^2\,(1+\cos\theta_2) + 2\cos\theta_{\mathrm{c}} r_3^2\,(1+\cos\theta_3) - 2\left(R_1^2+R_2^2\right)\right]$$

A given encapsulated droplet is not able to access every point in the $(\theta_1, \theta_2, \theta_3)$ space, because of two types of constraints: edge matching, which yields two equations:

$$r_1 \sin\theta_1 = r_2 \sin\theta_2; \tag{12}$$

$$r_2 \sin\theta_2 = r_3 \sin\theta_3, \tag{13}$$

and volume conservation, which yields a further two equations:

$$16R_1^3 = r_1^3\,\alpha(\theta_1) - r_2^3\,\alpha(\theta_2)\,; \tag{14}$$

$$16R_2^3 = r_2^3\,\alpha(\theta_2) + r_3^3\,\alpha(\theta_3)\,. \tag{15}$$

The approach we take to impose these four constraints is to eliminate as many variables as possible by substitution. There are four independent constraining equations involving six variables (the r_i and θ_i; R_1 and R_2 are given constants), so after combining them we should be left with $6 - 4 = 2$ free variables. The choice of variables to be left free is arbitrary; it was found that leaving θ_2 and θ_3 free allowed straightforward numerical solution of the equations, and relatively clear visualization of the results.

We first eliminate r_2 and r_3 by rearranging Eqs. 12 and 13 to give:

$$r_2 = r_1\frac{\sin\theta_1}{\sin\theta_2} \quad \text{and} \quad r_3 = r_2\frac{\sin\theta_2}{\sin\theta_3}.$$

Substituting the first of these into the second, we obtain r_2 and r_3 in terms of r_1 and the θ_i:

$$r_2 = r_1\frac{\sin\theta_1}{\sin\theta_2} \tag{16}$$

$$r_3 = r_1\frac{\sin\theta_1}{\sin\theta_3}. \tag{17}$$

Substituting these into the volume conservation equations, Eqs. 14 and 15, we obtain:

$$16R_1^3 = r_1^3 \left[\alpha(\theta_1) - \left(\frac{\sin\theta_1}{\sin\theta_2} \right)^3 \alpha(\theta_2) \right]; \tag{18}$$

$$16R_2^3 = r_1^3 \left[\left(\frac{\sin\theta_1}{\sin\theta_2} \right)^3 \alpha(\theta_2) + \left(\frac{\sin\theta_1}{\sin\theta_3} \right)^3 \alpha(\theta_3) \right]. \tag{19}$$

Now we rearrange the first of these to obtain r_1 (cubed) in terms of θ_1 and θ_2:

$$r_1^3 = \frac{16R_1^3}{\alpha(\theta_1) - \left(\frac{\sin\theta_1}{\sin\theta_2} \right)^3 \alpha(\theta_2)} \tag{20}$$

We leave r_1 in the cubed form because we immediately substitute it into the last unused constraining equation, Eq. 19; after rearranging, one obtains:

$$\alpha(\theta_1) = \left(\frac{\sin\theta_1}{\sin\theta_2} \right)^3 \left[1 + \left(\frac{R_1}{R_2} \right)^3 \right] \alpha(\theta_2) + \left(\frac{\sin\theta_1}{\sin\theta_3} \right)^3 \left(\frac{R_1}{R_2} \right)^3 \alpha(\theta_3) \,. \tag{21}$$

This equation allows us to calculate $\alpha(\theta_1)$ from given values of θ_2 and θ_3. Although it is not analytically tractable to calculate θ_1 from Eq. 21, this is easily done by numerical methods with a computer.

The procedure to create a free energy landscape is then as follows:

1. Choose values for R_1, R_2, γ_m and θ_c. The first two quantities are experimental variables, determined by the choice of oil drop and aqueous droplet volumes, while the latter two quantities depend only on the fluid and lipid compositions. All four quantities are kept constant throughout the procedure.

2. Choose values for θ_2 and θ_3 in the range of interest.

3. Calculate θ_1 using Eqs. 8 and 21, with the values chosen for θ_2 and θ_3. This was done with MATLAB's `fsolve` function.

4. Calculate r_1 using Eq. 20.

5. Calculate r_2 and r_3 using Eqs. 16 and 17.

6. Calculate ΔF using Eq. 3. This gives us the free energy of formation for an encapsulated droplet with the final shape dictated by the chosen values for θ_2 and θ_3.

7. Repeat from step 2, with different values of θ_2 and θ_3.

A MATLAB program was written to perform these steps for θ_2 at 4° intervals between 0° and 248°, and for θ_3 at 4° intervals between 0° and 188°, to produce the map of free energy of bilayer formation shown in Fig. 2 of the main text. The values chosen for the parameters are given in the text. The value of $\gamma_\mathrm{b}/\gamma_\mathrm{m} = 0.68$ given in the main text was derived from measurements of θ_c for pairs of aqueous droplets joined by interface bilayers in bulk oil, using the equation derived in the Appendix. θ_c was measured as $70 \pm 6°$ (mean ± s.d., $n = 10$) using droplets of buffer containing 500 mM KCl, and a bulk oil 9:1 (v/v) mixture of silicone oil and hexadecane containing 0.1 mg ml^{-1} DPhPC.

Inspection of the formula for ΔF shows that for a given ratio γ_b/γ_m, the absolute values of γ_m and γ_b affect only the energy scale of the free energy landscape, but not its shape. It follows that the equilibrium geometry of a multisome can be calculated given only the ratio of oil drop and aqueous droplet volumes, and the ratio γ_b/γ_m. Conversely, if a particular equilibrium geometry is desired, a similar analysis could impose design constraints on the relative droplet volumes and surface tensions.

1.5 Appendix

1.5.1 Buoyancy forces compared to surface tension forces

The magnitude of the buoyancy force on an aqueous droplet in an oil drop is $F_b = (\rho_a - \rho_o)\, g V_d$, where ρ_o and ρ_a are the densities of the oil drop and aqueous droplets, respectively, $g = 9.81\,\mathrm{m\,s^{-2}}$ and V_d is the droplet volume. We assume that $\rho_a = 1.05\,\mathrm{mg\,ml^{-1}}$, $\rho_o = 1.01\,\mathrm{mg\,ml^{-1}}$, and that the aqueous droplet has a radius of 200 μm. Inserting these values into the equation gives a buoyancy force of $F_b = 13\,\mathrm{nN}$.

A characteristic value for the surface tension forces may be calculated by integrating one of the surface tensions along the circle defined by the intersection of the two monolayers and the bilayer. As an example, we consider the monolayer between the aqueous droplet and the oil drop. Assuming a monolayer surface tension of $5\,\mathrm{mN\,m^{-1}}$ [16, 17], a typical circular radius of $200\,\mu$m and a contact angle of 173° as in the main text, we obtain a resultant vertical force of $\sim$770 nN, $\sim$60 times greater than the buoyancy force F_b.

1.5.2 Area of a spherical cap

Consider a spherical cap, or truncated sphere, of radius R (Fig. 4); we wish to find the area of its curved surface. To do this, we first find the curved surface area of the volume element shown in blue in the figure.

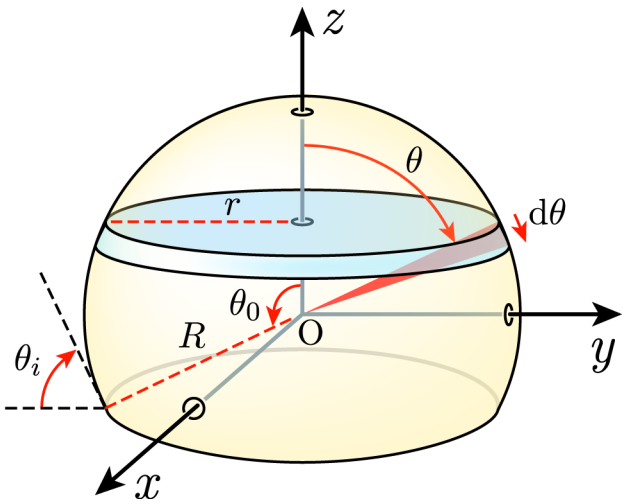

Figure 4: Geometrical definitions for the calculation of the curved area and volume of a spherical cap of radius R.

A horizontal disc whose circumference is at an angle θ from the z-axis has radius $r = R\sin\theta$, so that the circumference of the volume element is $2\pi R\sin\theta$. An arc on the sphere perpendicular to this circumference, subtending an infinitesimal angle $\mathrm{d}\theta$ at the origin (shown in red on the figure), has length $R\,\mathrm{d}\theta$. The curved area of the volume element is simply the product of these

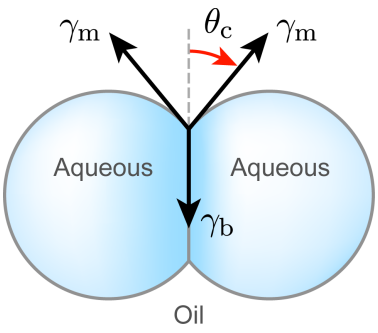

Figure 5: Surface tensions acting on a short line segment at the interface between the oil phase and the two aqueous droplets. θ_c is the droplet interface bilayer contact angle.

two lengths, $2\pi R^2 \sin\theta \, \mathrm{d}\theta$. The area of the entire curved surface of the spherical cap is then the integral of this area element over the range of θ subtended by the truncated sphere:

$$A = \int_0^{\theta_0} 2\pi R^2 \sin\theta \, \mathrm{d}\theta$$

$$\implies A = 2\pi R^2 \left(1 - \cos\theta_0\right)$$

As shown in Fig. 4, the contact angles θ_i defined in Fig. 1 are related to θ_0 by $\theta_i = \pi - \theta_0$, so that the curved surface area of a spherical cap with contact angle θ_i and radius of curvature r_i is

$$A_i = 2\pi {r_i}^2 \left(1 + \cos\theta_i\right). \tag{22}$$

1.5.3 Contact angle in a droplet interface bilayer in bulk oil

Equivalent to its definition as an energy cost per unit area, surface tension can also be seen as a force per unit length that acts in the plane of the surface. Consider the circle around a droplet interface bilayer in bulk oil, defined by the region where the two aqueous phases simultaneously meet the oil phase and each other. The sum of surface tensions acting at each infinitesimal line element on this circle must balance at equilibrium [18]. Referring to Fig. 5, balancing the vertical components of the monolayer and bilayer surface tensions gives:

$$\gamma_b = 2\gamma_m \cos\theta_c. \tag{23}$$

The ratio of the bilayer and monolayer surface tensions can therefore be expressed in terms of the easily measured contact angle of a droplet interface bilayer in bulk oil.

1.5.4 Volume of a spherical cap

Here we wish to find the volume of the truncated sphere shown in Fig. 4, and we use the volume element shown in blue as the element of integration. From the calculation of the area of a spherical cap, we know that the circular end of the volume element has area $\pi r^2 = \pi R^2 \sin^2\theta$. It may be shown that the infinitesimal height of the volume element is $R\sin\theta \, \mathrm{d}\theta$. The volume of the element is simply the product of the circular area and the infinitesimal height: $\pi R^3 \sin^3\theta \, \mathrm{d}\theta$.

The volume of the truncated sphere is then given by the following integral:

$$V = \int_0^{\theta_0} \pi R^3 \sin^3\theta \, \mathrm{d}\theta$$

$$\implies V = \frac{\pi R^3}{12} \left(8 + \cos 3\theta_0 - 9\cos\theta_0\right)$$

Expressed in terms of the parameters defined in Fig. 1, the volume of a truncated sphere with contact angle θ_i and radius of curvature r_i is

$$V_i = \frac{\pi {r_i}^3}{12} \left(8 - \cos 3\theta_i + 9\cos\theta_i\right). \tag{24}$$

2 Suspension of multisomes in the bulk aqueous phase

Multisomes were suspended within the bulk aqueous buffer from a small loop of silver wire or plastic, of diameter $\sim 0.8 - 1.5$ mm. Silver loops were made by wrapping 100-μm diameter silver wire around a cylindrical template. Plastic loops consisted of cross-sections cut from pipette tips. Each loop was then attached to a silver wire fixed to the container wall. Multisomes could be dislodged from silver loops by mechanical disturbance, whereas plastic loops held multisomes very reliably because of their strong adhesion to the oil drop.

3 Preparation of glass-sheathed electrodes

Glass-sheathed electrodes were made by threading 25-μm diameter silver wire through a glass capillary with internal and external diameters of 142 μm and 559 μm, respectively (Drummond). The capillary was then pulled (PC-10, Narishige) with the wire inside it, such that it separated into two pieces. The wire inside one of these pieces was soldered to an electrode pin at the larger opening of the capillary. Tweezers were used to trim $\sim 50\,\mu$m of glass from the pulled end of the capillary, exposing the end of the wire. This end was then treated with sodium hypochlorite solution as described in the Methods of the main text. A region near the pulled end of the capillary was coated with silicone rubber (3140 RTV Coating, Dow Corning) to prevent current leakage between the inner droplet and the external aqueous solution (Fig. 3a of main text).

References

[1] Holden, M. A., Needham, D. & Bayley, H. Functional bionetworks from nanoliter water droplets. *J. Am. Chem. Soc.* **129,** 8650–8655 (2007).

[2] Naraghi, M. T-jump study of calcium binding kinetics of calcium chelators. *Cell Calcium* **22,** 255–268 (1997).

[3] Johnson, J. D. Jiang, Y. & Rall, J. A. Intracellular EDTA mimics parvalbumin in the promotion of skeletal muscle relaxation. *Biophys. J.* **76,** 1514–1522 (1999).

[4] Akashi, K., Miyata, H., Itoh, H. & Kinosita, K., Jr. Preparation of giant liposomes in physiological conditions and their characterization under an optical microscope. *Biophys. J.* **71,** 3242–3250 (1996).

[5] Korlach, J., Schwille, P., Webb, W. W. & Feigenson, G. W. Characterization of lipid bilayer phases by confocal microscopy and fluorescence correlation spectroscopy. *Proc. Natl. Acad. Sci. USA* **96,** 8461–8466 (1999).

[6] Lindsey, H., Petersen, N. O. & Chan, S. I. Physicochemical characterization of 1,2-diphytanoyl-*sn*-glycero-3-phosphocholine in model membrane systems. *Biochim. Biophys. Acta* **555,** 147–167 (1979).

[7] Ueno, M., Yoshida, S. & Horikoshi, I. Characteristics of the membrane permeability of temperature-sensitive liposome. *B. Chem. Soc. Jpn.* **64,** 1588–1593 (1991).

[8] Unezaki, S. *et al.* Enhanced delivery and antitumor activity of doxorubicin using long-circulating thermosensitive liposomes containing amphipathic polyethylene glycol in combination with local hyperthermia. *Pharm. Res.* **11,** 1180–1185 (1994).

[9] Lichtenberg, D. *et al.* Effect of surface curvature on stability, thermodynamic behavior, and osmotic activity of dipalmitoylphosphatidylcholine single lamellar vesicles. *Biochemistry* **20,** 3462–3467 (1981).

[10] Zimmerberg, J. & Kozlov, M. M. How proteins produce cellular membrane curvature. *Nat. Rev. Mol. Cell Biol.* **7,** 9–19 (2006).

[11] Okushima, S., Nisisako, T., Torii, T. & Higuchi, T. Controlled production of monodisperse double emulsions by two-step droplet breakup in microfluidic devices. *Langmuir* **20,** 9905–9908 (2004).

[12] Chu, L. Y., Utada, A. S., Shah, R. K., Kim, J. W. & Weitz, D. A. Controllable monodisperse multiple emulsions. *Angew. Chem. Int. Edit.* **46,** 8970–8974 (2007).

[13] Seo, M., Paquet, C., Nie, Z., Xu, S. & Kumacheva, E. Microfluidic consecutive flow-focusing droplet generators. *Soft Matter* **3,** 986–992 (2007).

[14] Shum, H. C., Zhao, Y., Kim, S. H. & Weitz, D. A. Multicompartment polymersomes from double emulsions. *Angew. Chem. Int. Edit.* **50,** 1648–1651 (2011).

[15] Kusumaatmaja, H., Li, Y., Dimova, R. & Lipowsky, R. Intrinsic contact angle of aqueous phases at membranes and vesicles. *Phys. Rev. Lett.* **103,** 238103 (2009).

[16] Yue, B. Y., Jackson, C. M., Taylor, J. A. G., Mingins, J. & Pethica, B. A. Phospholipid monolayers at non-polar oil/water interfaces. Part 1 – Phase transitions in distearoyl-lecithin films at the *n*-heptane aqueous sodium chloride interface. *J. Chem. Soc. Farad. Trans. 1* **72,** 2685–2693 (1976).

[17] Morisaku, T., Yui, H. & Sawada, T. Development of a new experimental system for monitoring biomembrane reactions: combination of laser spectroscopic techniques and biomembrane models formed at an oil/water interface. *Anal. Sci.* **20,** 1605–1608 (2004).

[18] Aronson, M. P. & Princen, H. M. Contact angles associated with thin liquid-films in emulsions. *Nature* **286,** 370–372 (1980).

Additional figures

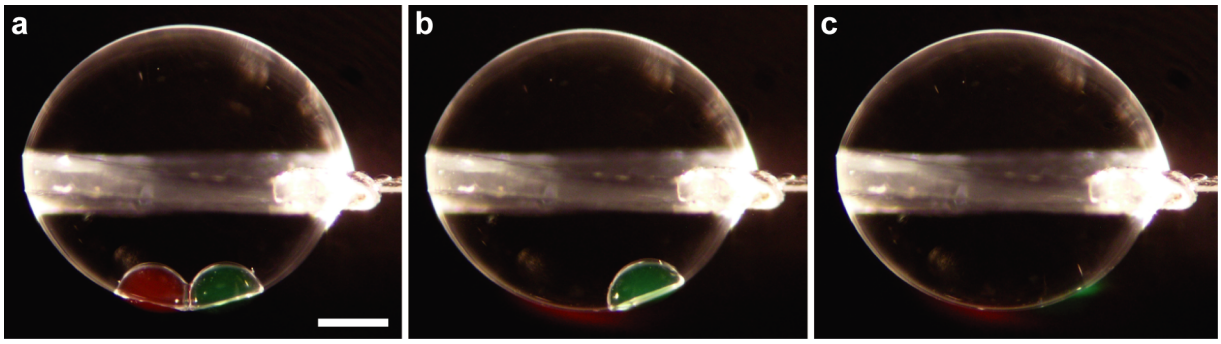

Figure S1: pH-dependent release of encapsulated contents into the aqueous environment. Photographs of a multisome with two inner droplets, made with a 2:1 (mol/mol) mixture of DOPE and OA. The red and green inner droplets contain 25 μM sulphorhodamine 101 and fluorescein, respectively. **a**, Multisome in pH 8.0 buffer. Exchange of the external buffer with buffer of the same pH had no effect. **b**, Bursting of one inner droplet upon lowering the pH of the external buffer to ~5.5. **c**, Bursting of the other inner droplet ~5 s after the first. Scale bar = 500 μm.